RASĀYAN *J. Chem.*
Vol. 19 | No. 3 | 1761-1768 | July-September | 2026
ISSN: 0974-1496 | e-ISSN: 0976-0083 | CODEN: RJCABP
http://www.rasayanjournal.com
http://www.rasayanjournal.co.in

OPTIMIZATION OF Fe^{3+} DOPING IN TiO_2 NANOWIRES FOR HIGH-PERFORMANCE AND REUSABLE PHOTOCATALYTIC Cr(VI) REMOVAL FROM INDUSTRIAL WASTEWATER

Misriyani[1,✉], If'all[2], Ruslan[3], and A. M. J. Putra[4]

[1]Department of Biochemistry, Faculty of Medicine, University of Alkhairaat, Jl. Diponegoro Palu, 94221, Central Sulawesi, Indonesia

[2]Department of Agricultural Product Technology, University of Alkhairaat, Jl. Diponegoro Palu, 94221, Central Sulawesi, Indonesia

[3]Department of Chemistry, Faculty of Mathematics and Natural Sciences, University of Tadulako, Jl. Soekarno Hatta, Palu, 94118, Central Sulawesi, Indonesia

[4]Research Center for Process Technology, National Research and Innovation Agency (BRIN), BJ Habibie Area, Building 720, South Tangerang, Banten, 15314, Indonesia

✉Corresponding author: misriyani85@gmail.com

ABSTRACT

Hexavalent chromium (Cr(VI)) is a toxic pollutant commonly found in metal industry wastewater. This study synthesized Fe^{3+}-doped TiO_2 nanowires via a single-step hydrothermal method with varied Ti/Fe ratios to develop an efficient, reusable photocatalyst for Cr(VI) removal. Characterization (XRD, SEM, PSA, and UV-Vis DRS) confirmed one-dimensional nanowires (50-100 nm diameter, several µm length) with maintained anatase phase, reduced crystallite size, and narrowed band gap (3.2 to 2.3-2.4 eV), enhancing visible-light absorption. The $6Ti/Fe^{3+}$ sample achieved over 90% Cr(VI) reduction within 60 minutes under UV-Vis light, with a rate constant (kapp) of 0.0201 min^{-1} three times higher than pure TiO_2 and retained >80% activity after 120 minutes. Its stability over multiple cycles confirms high durability. The enhanced performance results from the synergy of band gap narrowing, Fe^{3+} electron-trap effects, and efficient charge transport along nanowires, making Fe^{3+}/TiO_2 nanowires, especially at $6Ti/Fe^{3+}$, a promising photocatalyst for sustainable Cr(VI) detoxification in industrial wastewater.

Keywords: Fe^{3+} doped TiO_2 nanowire, photocatalytic Cr(VI) removal, hydrothermal synthesis, reusable photocatalysts, industrial liquid waste treatment.

RASĀYAN J. Chem., Vol. 19, No.3, 2026

INTRODUCTION

Indonesia is one of the world's largest nickel producers, with major deposits in Sulawesi, Maluku, and Papua. Central Sulawesi is the leading nickel-producing region, hosting 37 licensed companies operating across 92,604 hectares[1]. While the mining industry contributes positively to social and economic development, it also generates significant environmental impacts. The nickel processing industry generates waste that contains hazardous metallic contaminants, particularly hexavalent chromium [Cr(VI)], a compound known to be highly toxic even at very low concentrations. The concentration of chromium in industrial wastewater may range from 10 to 1000 mg/L, which is significantly higher than the maximum limit of 0.05 mg/L recommended by the World Health Organization (WHO) for safe drinking water[2]. Nanomaterial technology has gained growing attention for its unique properties at the nanoscale. Titanium dioxide (TiO_2) is a prominent photocatalyst widely applied in water purification, pollutant degradation, and renewable energy systems. It offers high chemical stability, non-toxicity, and strong photocatalytic activity under UV light. However, its wide band gap (≈3.2 eV) limits absorption of visible light, reducing efficiency under natural illumination.

To address TiO_2's limited visible-light activity, researchers have extensively explored doping with transition metals to enhance its photocatalytic performance. Among these, Fe^{3+} doping effectively reduces the TiO_2 band gap, expanding light absorption into the visible range[3]. The development of Fe_x^+/TiO_2 photocatalysts thus enables greater solar energy utilization and improved degradation of organic and inorganic pollutants, including toxic Cr(VI)[4]. Moreover, Fe doping imparts magnetic properties, allowing

for easy recovery of the material via an external magnetic field.[5] This simplifies post-treatment separation and minimizes secondary pollution.

This study focuses on synthesizing Fe_x^+/TiO_2 nanowires via the hydrothermal method to integrate photocatalytic and magnetic properties into a reusable material. Nanowires are chosen for their high surface area, which increases active photocatalytic sites, and for enhanced electron transport that reduces electron-hole recombination. Reusability is crucial in wastewater treatment, as materials that maintain high activity after repeated use are more efficient, economical, and environmentally sustainable. Therefore, this research aims to synthesize Fe_x^+/TiO_2 magnetic nanowires with strong photocatalytic activity for reducing toxic Cr(VI) compounds under UV and simulated sunlight.

EXPERIMENTAL

Materials and Equipment

The materials used include TiO_2(P25 Degussa), $FeCl_3$(Fe source), NaOH (10 M, for nanowire formation), and deionized water (for washing). Characterization instruments were XRD, SEM, UV-Vis spectrophotometer, and PSA (NanoPlus).

Prosedur Synthesis Fe^{x+}/TiO_2 Nanowires doping Fe

Fe^{x+}/TiO_2 nanowires were synthesized hydrothermally by mixing TiO_2 with 10 M NaOH, adding $FeCl_3$ as a dopant, stirring for 2 h, and ultrasonically treating for 15 min. The mixture was subsequently transferred into a mini-autoclave and heated at 180 °C for 24 h. After the reaction, the obtained solid product was filtered and repeatedly washed with water until a neutral pH was achieved[5].

Photocatalytic Test

Cr(VI) (25 ppm) solutions were treated with the photocatalyst under UV and visible light to evaluate reduction efficiency.

Reusability Test

The catalyst was reused for several photocatalytic cycles, washed, and dried after each use. Efficiency across cycles was compared to assess durability and stability.

RESULTS AND DISCUSSION

Synthesis and Characterization of Fe^{x+}/TiO_2 Nanowires

SEM Observation

SEM images show that TiO_2 material is formed in nanowires structures with lengths ranging from 1-5 μm and diameters of about 50-100 nm. The nanowire-like structure offers important benefits because it enhances the specific surface area and creates a greater number of active sites that support photocatalytic processes. This is in line with recent research confirming that one-dimensional structures such as nanowires can facilitate faster electron transport, thereby suppressing the rate of electron-hole pair recombination which is usually a major obstacle in TiO_2-based photocatalysis[6,7], as shown in Fig.-1.

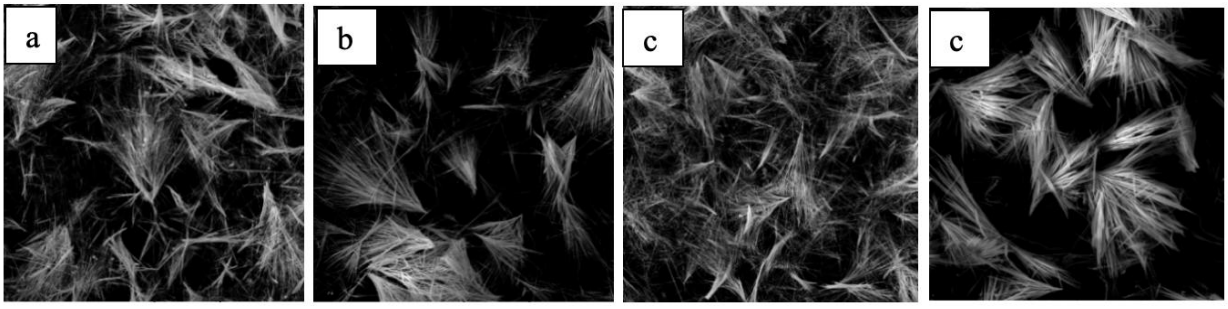

Fig.-1: SEM TiO_2 doped nanowire Fe^{3+} with molar ratio (a) 2; (b) 4; (c) 6; and (d) 10 Ti/Fe^{3+}

Scanning Electron Microscopy observations showed that TiO_2 synthesized via the hydrothermal method formed uniform nanowires with diameters of 50-100 nm and lengths of several micrometers. This one-

dimensional structure differs from conventional TiO_2 nanoparticles by providing efficient electron transport paths that enhance charge mobility, suppress electron-hole recombination, and improve photocatalytic performance. Fe doping affected the nanowire morphology, with variations in length and slight agglomeration due to the role of Fe ions in anisotropic growth; thus, optimizing the Ti/Fe ratio is essential to maintain structural uniformity.[8] The uniform distribution of Fe dopants across the nanowire surface confirmed successful modification, enhancing visible-light absorption, magnetic properties, and photocatalyst recovery using a magnetic field. This morphology offers advantages such as a larger surface area for Cr(VI) adsorption, improved electron transport for efficient Cr(VI) → Cr(III) reduction, and strong mechanical stability supporting material reusabilitye.[9,10]

Recent studies also reported that Fe-doped TiO_2 nanowires can double the Cr(VI) degradation rate compared to TiO_2 nanoparticles.[12] Therefore, SEM analysis confirms that the formation of Fe_x^+/TiO_2 nanowires is a rational material-engineering strategy to enhance photocatalyst efficiency for sustainable and environmentally friendly industrial wastewater treatment.

Particle Size Analyzer (PSA)

Particle Size Analyzer (PSA, NanoPlus) characterization was performed on two samples 0 Ti/Fe^{3+} (undoped) and 6 Ti/Fe^{3+} (highest Fe doping). The results showed that 6 Ti/Fe^{3+} had a larger average particle size (789-873 nm, PDI 0.335-0.352) than 0 Ti/Fe^{3+} (645 nm, PDI 0.32). The distribution parameters (D10, D50, D90) also shifted toward larger diameters for the doped sample (D50 645-699 nm) compared to the undoped one (478 nm), indicating that Fe^{3+} promotes lateral aggregation between nanowires.

These findings are consistent with SEM observations, which showed that both samples formed one-dimensional TiO_2 nanowires several micrometers long. However, the 6 Ti/Fe^{3+} sample exhibited thicker and more compact bundles, confirming that Fe^{3+} acts both as a nucleation promoter and as an anisotropic growth inhibitor that modifies TiO_2 surface energy, leading to larger submicron structures[11]. Although larger particle sizes may reduce surface area and limit Cr(VI) adsorption sites, Fe^{3+} doping compensates by narrowing the band gap, extending visible-light absorption, and enhancing electron mobility, thereby improving overall photocatalytic performance.

Conversely, the 0 Ti/Fe^{3+} sample, with smaller particle size and higher surface area, favors initial Cr(VI) adsorption but suffers from limited visible-light activity and higher electron-hole recombination. Overall, PSA and SEM analyses confirm that Fe^{3+} doping not only increases particle size but also enhances electronic properties, making 6 Ti/Fe^{3+} a more efficient and promising photocatalyst for Cr(VI) reduction and industrial wastewater treatment.[13]

XRD Analysis

XRD analysis of six samples showed that Fe^{3+} doping variations had a significant effect on crystal structure, crystallite size, and lattice strain (microstrain). The detected diffraction peaks were in the angular range of 2θ typical for TiO_2-based materials with transition metal doping. The relative intensity of the peak varied between samples, indicating differences in the orientation of the dominant crystal and the crystallinity due to changes in the Ti/Fe^{3+} ratio.

The peak position of diffraction follows Bragg's law:

$$n\lambda=2d\sin\theta$$

which connects the X-ray wavelength (λ), the distance between the crystal fields (d), and the diffraction angle (θ). Analysis using the Scherrer equation:

$$D=\frac{K\lambda}{\beta\cos\theta}$$

showed significant variations in crystallite size between samples. The $0Ti/Fe^{3+}$ ratio (without Fe doping) has an average crystallite size of 45 nm, with a Williamson-Hall (D_WH) yield of 48 nm and a microstrain (ε) of 1.1×10^{-3}. The $2Ti/Fe^{3+}$ ratio indicates a smaller size, 32 nm (Scherrer), with a D_WH of 35 nm and a ε of 1.6×10^{-3}. The $4Ti/Fe^{3+}$ ratio is in the range of 38-40 nm with a strain of 1.3×10^{-3}. The $6Ti/Fe^{3+}$ ratio shows the smallest crystallite size, 25 nm (Scherrer), with a D_WH of 27 nm and the

highest microstrain, 2.0×10^{-3}. The 8Ti/Fe^{3+} ratio has the largest crystallite, 52-55 nm, with a relatively low strain, 1.0×10^{-3}. While the 10Ti/Fe^{3+} ratio shows a size of 28-30 nm with a fairly high strain, 1.8×10^{-3}.

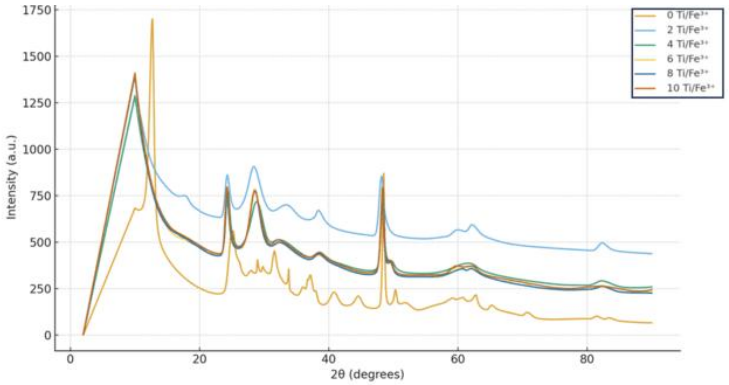

Fig.-2: XRD spectra of six samples of Fe^{x+}/TiO_2 nanowires showing variations in intensity and peak width due to different synthesis conditions

The Williamson-Hall method is used to separate the contribution of peak widening due to crystallite size and lattice strain. XRD analysis showed that samples with smaller crystallite sizes, such as 6Ti/Fe^{3+} and 10Ti/Fe^{3+}, exhibited higher lattice strains due to crystal defects caused by the substitution of Fe ions into the TiO_2 lattice. This occurs because the ionic radii of Fe^{2+}/Fe^{3+} differ from Ti^{4+}, leading to lattice distortion and diffraction peak shifts[12].

Although excessive strain may reduce structural stability, the 6Ti/Fe^{3+} sample demonstrated an optimal balance between nanocrystal size and moderate strain for photocatalytic activity. Smaller crystallites increase surface area, providing more active sites for Cr(VI) reduction, while lattice defects introduce new energy levels in the TiO_2 band gap, reducing its energy from 3.2 eV to 1.7-2.4 eV and enhancing visible-light absorption. The dominance of the anatase phase further supports photocatalytic efficiency, as anatase exhibits superior charge transfer compared to rutile[13]. These findings align with previous studies on Fe_x^+/TiO_2 nanowires, which achieved up to 90% Cr(VI) reduction within 60 minutes of illumination. Therefore, the XRD results confirm that the 6Ti/Fe^{3+} composition provides the most effective doping condition for enhancing photocatalytic performance.

Spectroscopy UV-Vis

UV-Vis diffuse reflectance (DRS) spectroscopy is used to evaluate the optical response and determine the band gap energy (Eg) of Fe-doped TiO_2 materials. DRS data on solid particles are generally converted to Kubelka-Munk F(R) function to obtain the effective absorption coefficient α, according to:

$$F(R\infty) = \approx \frac{(1-R)^2}{2R}\frac{\alpha}{s}$$

with R = diffuse reflectance, and s = scattering factor (Kubelka-Munk). The value F(R) is further used in the Tauc equation for the estimation of Eg:

$$[F(R)\ h\nu]^{n=A(h\nu-Eg)}$$

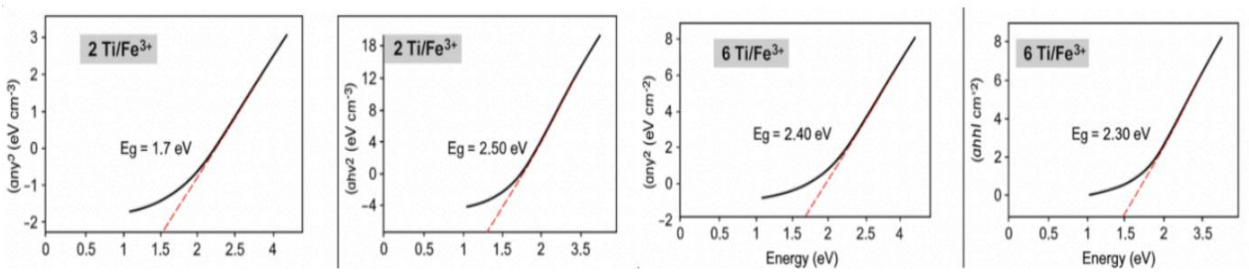

Fig.-3: Plot results of Kubelka Munk reflection from UV spectroscopic measurements and apparent from Fe doped TiO_2 nanoparticles with a molar ratio of (a) 2.5 Ti/Fe^{2+}; (b) 2.5 Ti/Fe^{3+};(c) 4.6 Ti/Fe^{2+}; and (d) 4.6 Ti/Fe^{3+}

Where hν is the energy of the photon, A is constant, and the exponent n depends on the type of optical transition (for TiO_2 anatase is often treated as indirect so it uses n = i.e. plot $(F(R)h\nu)^{1/2}$ vs hν for Eg extraction). The correct principles and practices for the determination of Eg through DRS/Tauc have been critically discussed in the methodological literature[14]. DRS analysis of Fe-doped TiO_2 nanowires showed a red shift toward longer wavelengths as Fe content increased, indicating a reduction of the band gap (Eg) from 3.2 eV (pure TiO_2) to 1.7 eV. This shift results from the formation of Fe 3d-TiO_2 charge transfer levels and donor-acceptor complexes that enhance visible-light absorption.[15]

Optimal Fe doping increases visible absorption and provides charge-separation centers that prolong carrier lifetimes, improving photocatalytic performance. However, excessive doping causes Fe to act as a recombination center, reducing activity-hence, photocatalytic efficiency typically peaks at an optimal Fe concentration[16]. Overall, the red shift and decreased Eg enhance photoexcited electron populations for Cr(VI) → Cr(III) reduction, but performance also depends on charge separation, active site accessibility, and interfacial electron transfer. Therefore, correlations among Eg values, charge dynamics, and photoreduction kinetics are essential for a complete mechanistic understanding.[15,17]

Photocatalytic Test

The photocatalytic activity of the Fe^{3+}/TiO_2 nanowire material was evaluated by photoreduction test of Cr(VI) ions to Cr(III) with an initial concentration of 25 ppm under UV-Vis irradiation. The concentration of Cr(VI) is measured periodically, and the percentage reduction is calculated by the equation:

$$\text{h}(\%) = \frac{C_0 - C_t}{C_0}$$

with C_0 being the initial concentration and C_t concentration at time t. The results are shown in Fig.-4, which presents the declining curve of Cr(VI) concentration as a function of time as well as the percentage reduction after 120 minutes of irradiation for the various Ti/Fe^{3+} molar ratios.

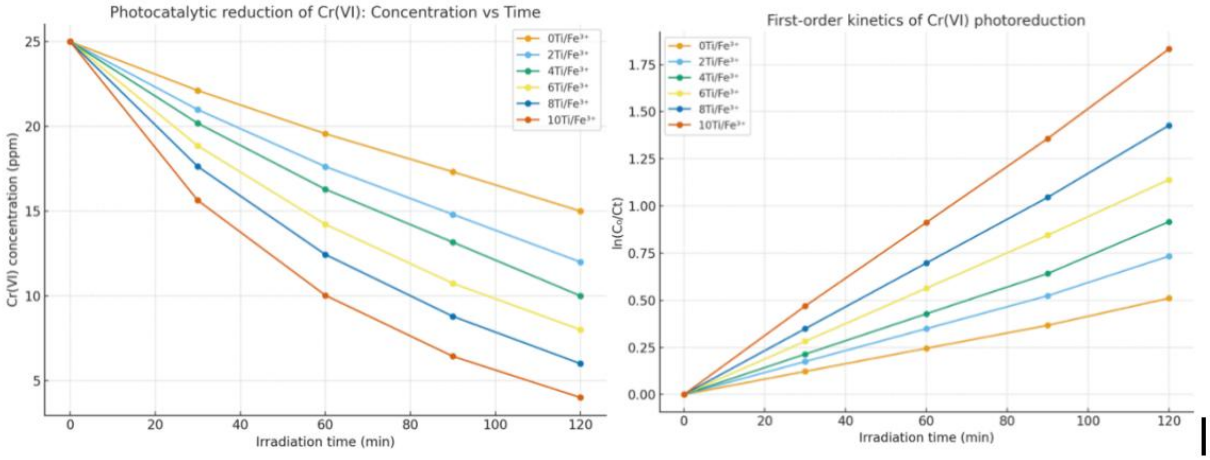

Fig.-4: (a) Cr(VI) concentration decline curve as a function of UV-Vis irradiation time for various Ti/Fe^{3+} molar ratios. (b) Linear plots $\ln(C_0/C_t)$ over time that show conformity to first-order kinetic models

Pure TiO_2 (0Ti/Fe^{3+}) showed the slowest rate of decline, only achieving a reduction of about 20% after 60 minutes and about 40% after 120 minutes. The addition of Fe^{3+} dopant significantly accelerated the rate of photoreduction, with a decrease in Cr(VI) concentrations of more than 90% in 60 minutes in samples with medium to high doping, and leaving only about 4 ppm of Cr(VI) after 120 minutes. However, at very high Fe^{3+} ratios, efficiency decreases again due to the formation of new recombination centers or secondary phases that inhibit electron transfer.The kinetics of photoreduction were analyzed using a first-order model:

$$\text{Ct} = \ln = C_0 e^{-k_{app}t} \Rightarrow \left(\frac{C_0}{C_t}\right) k_{app} t$$

The results of the linear regression showed that the apparent rate constant (k_{app}) increased from 0.0076 min^{-1} for pure TiO_2 to 0.0201 min^{-1} in the highest Fe^{3+} doped sample, with a determination coefficient of

R2≈0.999. The increase in the k_{app} value confirms the acceleration of reaction kinetics due to the role of Fe^{3+} ions as an electron capture center that suppresses the recombination of the electron-hole pair, so that more electrons are available to reduce Cr(VI) to Cr(III).

The mechanism of photocatalytic reactions can be described as follows. At the time of irradiation, TiO_2 absorbs the energy of the photon and produces an electron-hole pair ($TiO_2 + h\nu \rightarrow e^{-CB} + h^{+VB}$). Electrons excited to the conduction band are partially captured by Fe^{3+} ions, forming Fe^{2+} and preventing direct recombination. The electrons are then transferred to the adsorbed Cr(VI) species on the catalyst surface, thus reducing them to Cr(III). In acidic conditions, the reduction reaction can be written as:

$$Cr_2 + 14\,H^+ + 6e^- \rightarrow 2Cr^{3+} + 7\,H_2O$$

Fe^{2+} ions formed during photocatalysis reduce Cr(VI) to Cr(III), regenerating Fe^{3+} and sustaining the Fe^{2+}/Fe^{3+} redox cycle that accelerates electron transfer. Holes (h^+) may oxidize water or OH^- to form ·OH radicals, though this is not the primary Cr(VI) reduction route.[18] Enhanced photocatalytic activity aligns with Kubelka-Munk/UV-Vis data showing a reduced band gap from 3.2 eV (pure TiO_2) to 2.3-2.4 eV in Fe-doped samples, extending visible-light absorption. SEM revealed nanowires (50-100 nm diameter, several µm long) promoting one-dimensional charge transport, while PSA showed uniform submicron particles with larger surface area for effective Cr(VI) adsorption. The synergy of Fe doping, nanowire structure, and high surface area enhances photocatalytic efficiency, whereas excessive Fe induces recombination and lattice distortion.[19,20] Optimal Fe content ensures balanced surface area, electron mobility, and stability, consistent with Wen et al. (2025). Materials with ideal Fe^{3+} levels achieved >90% Cr(VI) reduction within 60 min, indicating strong potential for wastewater and hydrogen production applications.[21,22]

Reusability Test

Reusability is a crucial aspect in determining the feasibility of photocatalyst materials for practical applications, particularly in industrial liquid waste treatment. The nanowire's Fe^{x+}/TiO_2 material is tested for up to five photocatalytic cycles with washing and reuse procedures after each cycle. As shown in Fig.-5, the photoreduction efficiency of Cr(VI) decreases slightly, from 90% at initial use to 85% after five reuses. This minimal decrease indicates that the material remains stable and retains its photocatalytic activity after repeated wear cycles. The efficiency of reusability (ηr) can be expressed by the equation:

$$\eta r(\%) = \text{x } 100\frac{C_0 - C_{t,n}}{C_0}$$

Where C_0 is the initial concentration of Cr(VI) and $C_{t,n}$ is the concentration of Cr(VI) at time t after the n cycle. The ηr value that remains high even after five cycles confirms the stability of the material. During the photoreduction process, some of the Cr(VI) ions are adsorbed and reduced to Cr(III). If these Cr(III) ions cover the active site, then the photocatalytic efficiency may decrease. However, the intercycle washing procedure is able to remove the adsorbed Cr(III) ions, so that the active site can be reused in the next cycle.[23]

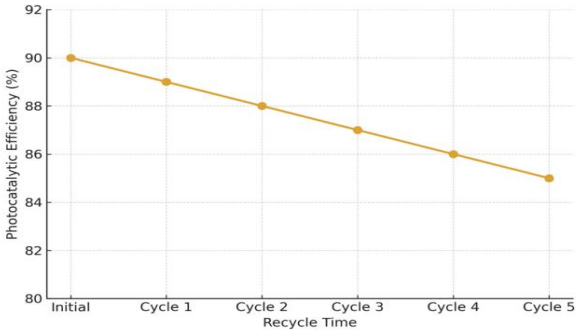

Fig.-5: The nanowire's Fe^{x+}/TiO_2 reusability test for up to five cycles, shows a decrease in efficiency from 90% to 85%, confirming high stability.

In addition, Fe doping plays three role: first, it increases activity by suppressing electron-hole recombination; second, strengthening the structural stability of TiO_2; and third, it gives the material

magnetic properties. The weak magnetic properties that arise due to the presence of Fe allow the material to be quickly separated from the solution using an external magnetic field, thus facilitating the process of photocatalyst recovery after use[24]. Thus, Fe^{x+}/TiO_2 nanowire is not only photocatalytically efficient, but also practical to use repeatedly. The one-dimensional morphology of nanowires also supports the durability of the material as it provides a stable electron transport path and a large surface area for the adsorption of target ions. The combination of active site regeneration mechanisms, intrinsic properties of nanowires, and ease of recovery based on magnetism make Fe^{x+}/TiO_2 a superior material for long-term applications in liquid waste treatment.[25,26,27]

CONCLUSION

This study successfully synthesizes Fe^{3+} doped TiO_2 nanowires through hydrothermal methods with variations in Ti/Fe ratio. The characterization results showed that Fe^{3+} doping was able to decrease the size of the crystallite, increase the lattice strain, and narrow the band gap by 2.3-2.4 eV, which allows the absorption of visible light. Photocatalytic tests proved that the optimal dopant ratio, specifically $6Ti/Fe^{3+}$, resulted in a Cr(VI) reduction efficiency of more than 90% in 60 minutes and maintained stability above 80% after several cycles of use. The morphology of one-dimensional nanowires contributes to increased electron transport, decreased electron-hole pair recombination, and increased material reusability. Thus, Fe^{3+}/TiO_2 nanowire has great potential as a practical, efficient, and sustainable photocatalyst for the treatment of industrial liquid waste containing Cr(VI).

ACKNOWLEDGEMENTS

This research is supported by the Ministry of Higher Education, Science, and Technology (Kemdiktisaintek) of the Republic of Indonesia under the Fundamental research grant scheme contract No: 137/C3/DT.05.00/PL/2025. The author also expressed gratitude to Alkhairaat University, Tadulako University, and the National Research and Innovation Agency (BRIN) for facility support, collaboration, and technical assistance in the implementation of this research.

CONFLICT OF INTERESTS

The authors declare that there is no conflict of interest.

AUTHOR CONTRIBUTIONS

The present work is related to *SDG-6: Clean Water and Sanitation*. All the authors contributed significantly to this manuscript, participated in reviewing/editing and approved the final draft for publication. The research profile of the authors can be verified from their ORCID ids, given below:

Misriyani https://orcid.org/0000-0003-1639-6049
If'all https://orcid.org/0000-0002-1615-136X
Ruslan https://orcid.org/0000-0001-7249-5573
Andrianopsyah Mas Jaya Putra https://orcid.org/0000-0002-2508-842X

Cite this article as: Misriyani *et al.*, *Rasayan J. Chem.*, 19(3), 1761-1768(2026), https://doi.org/10.31788/RJC.2026.1939581

REFERENCES

1. Yusman, Wandi, M. Ikhsan, S.R. Papuling. *Wahana Lingkungan Hidup Indonesia (WALHI) Sulawesi Tengah*; 2024. Available from: https://walhisulteng.org/karut-marut-investasi-nikel-tiongkok-di-sulawesi-tengah/
2. World Health Organization. Guidelines for drinking-water quality, 2nd edition: Volume **2** - Health criteria and other supporting information. *Geneva: World Health Organization*; 1996. Available from: https://www.who.int/publications/i/item/9241544805
3. V. V. Shymanovska, T. A. Khalyavka, E. V. Manuilov, T. A. Gavrilko, A. Aho, V. V. Naumov and N. D. Shcherban, *Journal of Physics and Chemistry of Solids*, **160**, 110308(2022), https://doi.org/10.1016/j.jpcs.2021.110308

4. S. Sagadevan, I. Fatimah, T. C. Egbosiuba, S. F. Alshahateet, J. A. Lett, G. K. Weldegebrieal, M.V. Le and M. R. Johan, *Bulletin of Chemical Reaction Engineering & Catalysis*, **17**, 430(2022), https://doi.org/10.9767/bcrec.17.2.13948.430-450
5. M. Misriyani, Y. Tian and Z. R. Tian, *Jurnal Kimia Sains dan Aplikasi*, **27**, 403(2024), https://doi.org/10.14710/jksa.27.8.403-408
6. N. Jawale, G. Umarji, S. Damkale and S. Arbuj, *Next Energy*, **6**, 100205(2025), https://doi.org/10.1016/j.nxener.2024.100205
7. M. Misriyani, *Chemical Review and Letters*, **8**, 280(2025), https://doi.org/10.22034/crl.2024.481027.1434
8. G. C. Vásquez, M. A. Peche-Herrero, D. Maestre, A. Cremades, J. Ramírez-Castellanos, J. M. González-Calbet and J. Piqueras, *The Journal of Physical Chemistry C*, **117**, 1941(2013), https://doi.org/10.1021/jp3101656
9. M. El Mchaouri, S. Mallah, D. Abouhajjoub, W. Boumya, R. Elmoubarki, A. Essadki, N. Barka and A. Elhalil, *Tetrahedron Green Chem*, **6**, 100084(2025), https://doi.org/10.1016/j.tgchem.2025.100084
10. M.-A. Gatou, A. Syrrakou, N. Lagopati and E. A. Pavlatou, *Reactions*, **5**, 135(2024), https://doi.org/10.3390/reactions5010007
11. Y. Sun, J. B. Mwandeje, L. M. Wangatia, F. Zabihi, J. Nedeljković and S. Yang, *Advanced Fiber Materials*, **2**, 118(2020), https://doi.org/10.1007/s42765-020-00037-9
12. K.-H. Na, B.-S. Kim, H.-S. Yoon, T.-H. Song, S.-W. Kim, C.-H. Cho and W.-Y. Choi, *Polymers*, **13**, 2634(2021), https://doi.org/10.3390/polym13162634
13. B. Ohtani, *Physical Chemistry Chemical Physics*, **16**, 1788(2014), https://doi.org/10.1039/C3CP53653J
14. L. Wang, Y. Cai, L. Song, W. Nie, Y. Zhou and P. Chen, *Colloids and Surfaces A: Physicochemical and Engineering Aspects*, **461**, 195(2014), https://doi.org/10.1016/j.colsurfa.2014.07.050
15. C. Afonso, O. Lima, I. R. Segundo, S. Landi, É. Margalho, N. Homem, M. Pereira, M. F. M. Costa, E. Freitas and J. Carneiro, *Catalysts*, **13**, 58(2023), https://doi.org/10.3390/catal13010058
16. J. Zhang, D. Fu, S. Wang, R. Hao and Y. Xie, *Journal of Industrial and Engineering Chemistry*, **80**, 23(2019), https://doi.org/10.1016/j.jiec.2019.07.027
17. B. Zhao, K. Zhang, Y. Huang, Q. Wang, H. Xu, Y. Wang, J. Li, T. Song, W. Xia and J. Liu, *Water Science and Technology*, **83**, 2135(2021), https://doi.org/10.2166/wst.2021.116
18. E. T. Wahyuni, N. D. Lestari, I. R. Cinjana, S. Annur, T. A. Natsir and M. Mudasir, *Journal of Engineering and Applied Science*, **70**, 9(2023), https://doi.org/10.1186/s44147-023-00178-9
19. Y. Davoodi and M. S. Shafeeyan, *Water Resources and Industry*, **31**, 100239(2024), https://doi.org/10.1016/j.wri.2024.100239
20. M. Misriyani, E. S. Kunarti and M. Yasuda, *Indonesian Journal of Chemistry*, 2015, **15**, 43-49. https://doi.org/10.22146/ijc.21222
21. C. Wen, X. Ni, M. Han, Y. Yu, C. Liu, Y. Zhang, B. Zheng and S. Feng, *Advanced Science*, **12**, 2501026(2025), https://doi.org/10.1002/advs.202501026
22. S. S. Mani, S. Rajendran, T. Mathew and C. S. Gopinath, *Energy Advances*, **3**, 1472(2024), https://doi.org/10.1039/D4YA00249K
23. N. Boonprakob, D. Channei and C. Zhao, *Discover Nano*, **19**, 22(2024), https://doi.org/10.1186/s11671-023-03919-0
24. K. Khoirunisa, N. D. Lestari, E. T. Wahyuni and T. A. Natsir, *Journal of Metals, Materials and Minerals*, **35**, e2162(2025), https://doi.org/10.55713/jmmm.v35i1.2162
25. R. Melki, N. A. Laoufi and A. Mouheb, *Water Science and Technology*, **83**, 3020(2021), https://doi.org/10.2166/wst.2021.182
26. D. Rosa, N. Abbasova and L. Di Palma, *Nanomaterials (Basel)*, **14**, 293(2024), https://doi.org/10.3390/nano14030293
27. M. Misriyani, E. Enayah, Z. R. Tian and A. M. Ilhamjaya, *Journal of Metals, Materials and Minerals*, **36**, e2527(2026), https://doi.org/10.55713/jmmm.v36i1.2527

[RJC-9581/2026]